

---

## Effect of Radiation on MHD Convection Flow Past a vertical Permeable Moving Plate

Murali Gundagani, NVN Babu

Department of Mathematics, GITAM University, Rudraram, India

---

### Article Info

#### Article history:

Received Jan 5, 2012

Revised Feb 23, 2012

Accepted Mar 1, 2012

#### Keyword:

FEM

Heat and Mass transfer

MHD

Radiation

---

### ABSTRACT

The paper examined the radiation effect on unsteady MHD free convection heat and mass transfer flow on a viscous, incompressible, electrically conducting fluid past a vertical permeable moving plate with radiation. The non-linear partial differential equations governing the flow have been solved numerically using finite element method. It has been observed that the velocity increases with the increase in the radiation parameter and there is an increase in temperature with the increase in the value of radiation parameter.

Copyright © 2012 Institute of Advanced Engineering and Science.  
All rights reserved.

---

### Corresponding Author:

**Murali Gundagani**

Department of Mathematics, GITAM University,  
Rudraram, India.

Email: muraligundagani@yahoo.in

---

## 1. INTRODUCTION

Radiation and on the optical properties of the emitter, with its internal energy being converted to is the process of heat propagation by means of electromagnetic waves, depending only on the temperature radiation energy. The process involving the convection of internal energy of the solution in to radiation energy is known as radiation heat transfer. In contrast to the mechanism of conduction and convection, where energy transfer through a material medium is involved, heat also be transferred through regions where a perfect vacuum exists. The mechanism in this case is electromagnetic radiation. The electromagnetic radiation which is propagated as a result of temperature differences, this is called thermal radiation.

The effect of radiation on MHD flow and heat transfer problem have become more important industrially. A high operating temperature, radiation effect can be quite significant. Many processes in engineering are as occur at high temperature and a knowledge of radiation heat transfer becomes very important for the design of the pertinent equipment. Nuclear power plants, gas turbines and the various propulsion devices for aircraft, missiles, satellites and space vehicles are examples of such engineering areas. Bestman [1] examined the natural convection boundary layer with suction and mass transfer in a porous medium. His results confirmed the hypothesis that suction stabilises the boundary layer and affords the most efficient method in boundary layer control yet known. Abdus Sattar and Hamid Kalim [2] investigated the unsteady free convection interaction with thermal radiation in a boundary layer flow past a vertical porous plate. Makinde [3] examined the transient free convection interaction with thermal radiation of an absorbing-emitting fluid along a moving vertical permeable plate. Recently, Ibrahim et al., [4] have studied nonclassical thermal effects in Stokes' second problem for micropolar fluids by using perturbation method.

Muthucumaraswamy and Ganesan [5] studied effect of the chemical reaction and injection on flow characteristics in unsteady upward motion of an isothermal plate. Dekaetal, [6] studied the effect of the first-order homogeneous chemical reaction on the process of an unsteady flow past an infinite vertical plate with a constant heat and mass transfer. Chamkha [7] studied the MHD flow of a numerical of uniformly stretched vertical permeable surface in the presence of heat generation/absorption and a chemical reaction. Soundalgekar and Patti [8] studied the problem of the flow past an impulsively started isothermal infinite vertical plate with mass transfer effects. The effect of foreign mass on the free-convection flow past a semi-infinite vertical plate were studied [9]. Chamkha [10] assumed that the plate is embedded in a uniform porous medium and moves with a constant velocity in the flow direction in the presence of a transverse magnetic field. Raptis [11] investigate the steady flow of a viscous fluid through a porous medium bounded by a porous plate subjected to a constant suction velocity by the presence of thermal radiation. Raptis and Perdikis [12] studied the unsteady free convection flow of water near a laminar boundary layer over a vertical moving porous plate.

Chambreet al [13] have analyzed a first order chemical reaction in the neighborhood of a stationary horizontal plate. Das et al [14] have studied the effect of homogeneous first order chemical reaction on the flow past an impulsively started infinite vertical plate with uniform heat flux and mass transfer. Again, mass transfer effects on moving isothermal vertical plate in the presence of chemical reaction studied by Das et al [15]. The dimensionless governing equations were solved by the usual Laplace-transform technique and the solutions are valid only at lower time level. Radiation and chemical reaction effects on isothermal vertical oscillating plate with variable mass diffusion has been studied by Manivannan et al [16].

In spite of all the studies, the heat and mass transfer effects on unsteady magneto hydrodynamic free convection flow past a vertical permeable moving plate with radiation.

## 2. MATHEMATICAL ANALYSIS

Consider unsteady two-dimensional flow of a laminar, viscous, electrically conducting and heat-absorbing fluid past a semi-infinite vertical permeable moving plate embedded in a uniform porous medium and subjected to a uniform transverse magnetic field in the presence of thermal and concentration buoyancy effects. It is assumed that there is no applied voltage which implies the absence of an electric field. The fluid properties are assumed to be constant except that the influence of density variation with temperature has been considered only in the body-force term. The concentration of diffusing species is very small in comparison to other chemical species, the concentration of species far from the wall,  $C_\infty$ , is infinitely small [5] and hence the Soret and Dufour effects are neglected. The chemical reactions are taking place in the flow and all thermophysical properties are assumed to be constant of the linear momentum equation which is approximated according to the Boussinesq approximation. Due to the semi-infinite plane surface assumption, the flow variables are a function of  $y^*$  and  $t^*$  only. Under the above assumptions, the equations that describe the physical situation are given by

$$\frac{\partial v^*}{\partial y^*} = 0, \quad (1)$$

$$\frac{\partial u^*}{\partial t^*} + v^* \frac{\partial u^*}{\partial y^*} = \nu \frac{\partial^2 u^*}{\partial y^{*2}} - v^* \frac{u^*}{K'} - \frac{\sigma B_0^2 u^*}{\rho} + g\beta_T(T^* - T_\infty) + g\beta_C(C^* - C_\infty), \quad (2)$$

$$\frac{\partial T^*}{\partial t^*} + v^* \frac{\partial T^*}{\partial y^*} = \frac{k}{\rho c_p} \frac{\partial^2 T^*}{\partial y^{*2}} - \frac{1}{\rho c_p} \left( \frac{\partial q_r}{\partial y^*} \right) \quad (3)$$

$$\frac{\partial C^*}{\partial t^*} + v^* \frac{\partial C^*}{\partial y^*} = D \frac{\partial^2 C^*}{\partial y^{*2}} - K_r C^* \quad (4)$$

where  $x^*$ ,  $y^*$ , and  $t^*$  are the dimensional distances along and perpendicular to the plate and dimensional time, respectively.  $U^*$  and  $v^*$  are the components of dimensional velocities along  $x^*$  and  $y^*$  directions, respectively,  $T^*$  is the dimensional temperature,  $C^*$  is the dimensional concentration,  $C_w$  and  $T_w$  are the concentration and temperature at the wall, respectively.  $C_\infty$  and  $T_\infty$

are the free stream dimensional concentration and temperature, respectively.  $\rho$  is the fluid density,  $\nu$  is the kinematic viscosity,  $c_p$  is the specific heat at constant pressure,  $\sigma$  is the fluid electrical conductivity,  $B_0$  is the magnetic induction,  $K^*$  is the permeability of the porous medium,  $Q_1^*$  is the coefficient of proportionality for the absorption of radiation,  $D$  is the mass diffusivity,  $g$  is the gravitational acceleration, and  $\beta_T$  and  $\beta_c$  are the thermal and concentration expansion coefficients, respectively and  $K_l$  is the chemical reaction parameter. The magnetic and viscous dissipations are neglected in this study. The third and fourth terms on the RHS of the momentum equation (2) denote the thermal and concentration buoyancy effects, respectively. Also, the second and third terms on the RHS of the energy equation (3) represents the heat and radiation absorption effects, respectively. It is assumed that the permeable plate moves with a variable velocity in the direction of fluid flow. In addition, it is assumed that the temperature and the concentration at the wall as well as the suction velocity are exponentially varying with time.

Under these assumptions, the appropriate boundary conditions for the velocity, temperature and concentration fields are

$$\left. \begin{aligned} u^* &= u_p^*, T^* = T_w + \varepsilon(T_w - T_\infty)e^{n^*t}, C^* = C_w + \varepsilon(C_w - C_\infty)e^{n^*t}, y^* = 0, \\ u^* &= 0, T^* \rightarrow T_\infty, C^* \rightarrow C_\infty, y^* \rightarrow \infty \end{aligned} \right\} \tag{5}$$

where  $u_p^*$  is the wall dimensional velocity,  $n^*$  is constant. It is clear from Eq. (1) that the suction velocity at the plate surface is a function of time only. Assuming that it takes the following exponential form:

$$v^* = -V_0(1 + \varepsilon A e^{n^*t}), \tag{6}$$

where  $A$  is areal positive constant,  $\varepsilon$  and  $\varepsilon A$  are small less than unity, and  $V_0$  is a scale of suction velocity which has non-zero positive constant. Introducing the dimensionless quantities:

$$\left. \begin{aligned} u &= \frac{u^*}{V_0}, v = \frac{v^*}{V_0}, y = \frac{V_0 y^*}{\nu}, t = \frac{V_0^2 t^*}{\nu}, u_p = \frac{u_p^*}{V_0}, n = \frac{n^* \nu}{V_0^2}, \theta = \frac{T^* - T_\infty}{T_w - T_\infty}, C = \frac{C^* - C_\infty}{C_w - C_\infty} \\ Gr &= \frac{\nu g \beta (T_w - T_\infty)}{V_0^3}, Gm = \frac{\nu g \beta_c (C_w - C_\infty)}{V_0^3}, Pr = \frac{\mu c_p}{k}, M^2 = \frac{\sigma \beta_0^2 \nu}{\rho V_0^2}, \\ K_0 &= \frac{K^* V_0^2}{\nu^2}, S_c = \frac{\nu}{D}, R = \frac{16 \sigma_s T_\infty^3}{3 K_e k}, K_r = \frac{K_r^* \nu}{V_0^2}, \end{aligned} \right\} \tag{7}$$

In view of the above non-dimensional variables, the basic field Eqs. (2)–(4) can be expressed in non dimensional form as

$$\frac{\partial u}{\partial t} - (1 + \varepsilon A e^{nt}) \frac{\partial u}{\partial y} = Gr \theta + Gm C + \frac{\partial^2 u}{\partial y^2} - \frac{u}{K_0 (1 + \varepsilon A e^{nt})} - M^2 u \tag{8}$$

$$\frac{\partial \theta}{\partial t} - (1 + \varepsilon A e^{nt}) \frac{\partial \theta}{\partial y} = \frac{1}{Pr} \frac{\partial^2 \theta}{\partial y^2} - R \theta \tag{9}$$

$$\frac{\partial C}{\partial t} - (1 + \varepsilon A e^{nt}) \frac{\partial C}{\partial y} = \frac{1}{Sc} \frac{\partial^2 C}{\partial y^2} - K_r C \tag{10}$$

The corresponding boundary conditions are

$$\left. \begin{aligned} u &= u_p, \theta = 1 + \varepsilon e^{nt}, C = 1 + \varepsilon e^{nt}, \text{ on } y = 0 \\ u &\rightarrow 0, \theta \rightarrow 0, C \rightarrow 0 \text{ as } y \rightarrow \infty, \end{aligned} \right\} \tag{11}$$

where  $Gr, Gm, M, K_0, Pr, R$  and  $Sc$  are the thermal Grashof number, solutal Grashof number, magnetic field parameter, permeability parameter, Prandtl number, radiation parameter and Schmidt number respectively.

The mathematical statement of the problem is now complete and embodies the solution of Eqs. (8)-(10) subject to boundary condition (11).

### 3. METHOD OF SOLUTION:

The set of differential Equations (8) to (10) subject to the boundary conditions (11) are highly nonlinear, coupled and therefore it cannot be solved analytically. Hence, following Reddy<sup>17</sup> and Bathe<sup>18</sup> the finite element method is used to obtain an accurate and efficient solution to the boundary value problem under consideration. The fundamental steps comprising the method are as follows:

**Step 1:** Discretization of the domain into elements:

The whole domain is divided into finite number of *sub-domains*, a process known as discretization of the domain. Each sub-domain is termed a *finite element*. The collection of elements is designated the *finite element mesh*.

**Step 2:** Derivation of the element equations:

The derivation of finite element equations i.e. algebraic equations among the unknown parameters of the finite element approximation, involves the following three steps:

- Construct the variational formulation of the differential equation.
- Assume the form of the approximate solution over a typical finite element.
- Derive the finite element equations by substituting the approximate solution into variational formulation.

**Step 3:** Assembly of element equations:

The algebraic equations so obtained are assembled by imposing the *inter-element* continuity conditions. This yields a large number of algebraic equations, constituting the *global finite element model*, which governs the whole flow domain.

**Step 4:** Impositions of boundary conditions:

The physical boundary conditions defined in equation (11) are imposed on the assembled equations.

**Step 5:** Solution of the assembled equations:

The final matrix equation can be solved by a direct or indirect (iterative) method. For computational purposes, the coordinate  $Y$  is varied from 0 to  $Y_{\max}$ , where  $Y_{\max}$  represents infinity i.e. external to the momentum, energy and concentration boundary layers. Numerical solutions for these equations are obtained by C-program. In order to prove the convergence and stability of finite element method, the same C-program was run with slightly changed values of  $h$  and  $k$ . This process is repeated until the desired accuracy of 0.0005 is obtained. Hence, the finite element method is stable and convergent.

The skin-friction, Nusselt number and Sherwood number are important physical parameters for this type of boundary layer flow.

The skin-friction at the plate, which in the non-dimensional form is given by

$$C_f = \frac{\tau'_w}{\rho U_0 V_0} = \left( \frac{\partial u}{\partial y} \right)_{y=0} \quad (12)$$

The rate of heat transfer coefficient, which in the non-dimensional form in terms of the Nusselt number is given by

$$Nu = -x \frac{\left( \frac{\partial T'}{\partial y'} \right)_{y'=0}}{T'_w - T'_\infty} \Rightarrow Nu Re_x^{-1} = - \left( \frac{\partial \theta}{\partial y} \right)_{y=0} \quad (13)$$

The rate of mass transfer coefficient, which in the non-dimensional form in terms of the Sherwood number, is given by

$$Sh = -x \frac{\left( \frac{\partial C'}{\partial y'} \right)_{y'=0}}{C'_w - C'_\infty} \Rightarrow Sh Re_x^{-1} = - \left( \frac{\partial C}{\partial y} \right)_{y=0} \quad (14)$$

Where  $Re_x = \frac{V_0 x}{\nu}$  is the local Reynolds number.

#### 4. RESULTS AND DISCUSSION:

Numerical evaluation of the analytical results reported in the previous section was performed and a representative set of results is reported graphically in figs.1-12. These results are obtained to illustrate the influence of the thermal Grashof number  $Gr$ , Solutal Grashof number  $Gm$ , magnetic parameter  $M$ , Permeability parameter  $K$ , thermal radiation  $R$ , Prandtl number  $Pr$ , Schmidt number  $Sc$  and chemical reaction parameter  $K_r$  on the velocity, temperature and the concentration profiles, while the values of the physical parameters are fixed at real constants

With

$$Gr = Gm = 2.0, M = 0.2, K = 0.5, Pr = 0.71, R = 1.0, Sc = 0.6, K_r = 0.5, A = 0.5, u_p = 0.5,$$

$\varepsilon = 0.2, n = 0.1, t = 1.0$  All graphs therefore correspond to these values unless specifically indicated on the appropriate graph.

Figure 1 presents typical velocity profiles in the boundary layer for various values of the thermal Grashof number  $Gr$ , while all other parameters are kept at some fixed values. The thermal Grashof number  $Gr$  defines the ratio of the species buoyancy force to the viscous hydrodynamic force. As expected, the fluid velocity increases and the peak value is more distinctive due to increase in the species buoyancy force. The velocity distribution attains a distinctive maximum value in the vicinity of the plate and then decreases properly to approach the free stream value.

The influence of the Solutal Grashof number  $Gm$  on the velocity is presented in Figure 2. The Solutal Grashof number signifies the relative effect of the thermal buoyancy force to the viscous hydrodynamic force in the boundary layer. As expected, it is observed that there is a rise in the velocity due to the enhancement of thermal buoyancy force. Here, the positive values of  $Gm$  correspond to cooling of the plate. Also, as  $Gm$  increases, the peak values of the velocity increases rapidly near the porous plate and then decays smoothly to the free stream velocity.

For different values of the magnetic field parameter  $M$ , the velocity profile are plotted in Figure 3. It is obvious that the effect of increasing values of the magnetic field parameter results in a decreasing velocity distribution across the boundary layer. Figure 4 illustrate the variation of velocity distribution across the boundary layer for various values of the permeability parameter  $K$ . The velocity increases with an increase in permeability parameter  $K$ .

Figures 5 and 6 illustrate the velocity and temperature profiles for different values of the Prandtl number  $Pr$ . The Prandtl number defines the ratio of momentum diffusivity to thermal diffusivity. The numerical results show that the effect of increasing values of Prandtl number results in a decreasing velocity (Fig 5). From Fig 6, it is observed that an increase in the Prandtl number results a decrease of the thermal boundary layer thickness and in general lower average temperature within the boundary layer. The reason is that smaller values of  $Pr$  are equivalent to increasing the thermal conductivities, and therefore heat is able to diffuse away from the heated plate more rapidly than for higher values of  $Pr$ . Hence in the case of smaller Prandtl numbers as the boundary layer is thicker and the rate of heat transfer is reduced.

For different values of the radiation parameter  $R$  the velocity and temperature profiles are plotted in Figures 7 and 8. It is obvious that an increase in the radiation parameter  $R$  results an increasing in the velocity and temperature profiles within the boundary layer, as well as an increasing in the momentum and thermal thickness. This is because the large  $R$  values correspond to an increased dominance of conduction over radiation thereby increasing buoyancy force (thus, vertical velocity) and thickness of the thermal and momentum boundary layers.

Figures 9 and 10 display the effects of the Schmidt number  $Sc$  on the velocity, temperature and concentration profiles, respectively. As the Schmidt number increases, the concentration decreases. This causes the concentration buoyancy effects to decrease yielding a reduction in the fluid velocity. The reduction in the velocity, temperature and concentration profiles are accompanied by simultaneous reductions in the momentum and concentration boundary layers thickness. These behaviors are clearly shown in Figs. 9 and 10.

Figures 11 and 12, displays results for the velocity and concentration distributions respectively. It is seen, that the velocity and concentration increases with decreasing the chemical reaction parameter  $K_r$ .

Also, we observe that the magnitude of the stream wise velocity increases and the inflection point for the velocity distribution moves further away from the surface.

## 5. CONCLUSION

The plate velocity was maintained at a constant value and the flow was subjected to a transverse magnetic field. The resulting partial differential equations were transformed into a set of ordinary differential equations using finite element method. Numerical results were performed and some graphical results were obtained to illustrate the details of the flow and heat and mass transfer characteristic and their dependence on some of the physical parameters. It was found that the velocity profiles increased due to decrease in chemical reaction parameter, the Schmidt number, magnetic field and Prandtl number parameters while it increased due to increases in thermal Grashof number, Solutal Grash of number, radiation parameter and Permeability parameters. However, an increase temperature profile is a function of an increase in radiation parameter while it decreased due to increases in Prandtl number. Also, it was found that the concentration profile increased due to decreases in the chemical reaction parameter and the Schmidt number.

## REFERENCES

- [1] Bestman AR. Natural convection boundary layer with suction and mass transfer in a porous Medium. *Int J Energy Res* 1990;14:389-96.
- [2] Abdusattar MD, Hamid Kalim MD. Unsteady free-convection interaction with thermal Radiation in a boundary layer flow past a vertical porous plate. *J Math PhysSci* 1996;30:25-37.
- [3] Makinde OD. Free convection flow with thermal radiation and mass transfer past a moving Vertical plate. *IntComm Heat Mass Transfer* 2005;32:1411-9.
- [4] Ibrihem FS, Hassanien IA, Bakr AA. Nonclassical thermal effects in stokes' second problem Formicropolar fluids. *ASME J ApplMech* 2005;72:468-74.
- [5] Muthucumaraswamy R, Ganesan P. Effect of the chemical reaction and injection on flow Characteristics in an unsteady upward motion of an isothermal plate. *J ApplMech Tech Phys* 2001;42:665-71.
- [6] Deka R, Das UN, Soundalgekar VM. Effect of mass transfer on flow past an impulsively Started infinite vertical plate with constant heat flux and chemical reaction. *ForschungimIngenieurwesen* 1994;60:284-7.
- [7] Chamkha AJ. MHD flow of a numerical of uniformly stretched vertical permeable surface in The presence of heat generation/absorption and a chemical reaction. *IntComm Heat Mass Trasfer* 2003;30:413-22.
- [8] Soundalgekar VM, Patti MR. Stokes problem for a vertical plate with constant heat flux. *Astrophys Space Sci* 1980;70:179-82.
- [9] Gebhart B, Pera L. The nature of vertical natural convection flow resulting from the Combined buoyancy effects of thermal and mass diffusion. *J Heat Mass Transfer* 1971;14:2025-50.
- [10] Chamkha AJ. Unsteady MHD convective heat and mass transfer past a semi-infinite vertical permeable moving plate with heat absorption. *Int J EngSci* 2004;42:217-30.
- [11] Raptis A. Radiation and free convection flow through a porous medium. *IntComm Heat Mass Transfer* 1998;25:289-95.
- [12] Raptis A, Perdikis C. Free convection flow of water near 4°C past a moving plate. *ForschungimIngenieurwesen* 2002;67:206-8.
- [13] Chambre PL, Young JD (1958). On the diffusion of a chemically reactive species in a laminar boundary layer flow, *The Physics of Fluids*, 1(1), pp. 48-54.
- [14] Das UN, Deka RK, Soundalgekar VM (1999). Effects of mass transfer on flow past an impulsively started infinite vertical plate with chemical reaction, *The Bulletin, GUMA*, 5(1), pp. 13-20.
- [15] Das UN, Deka RK, Soundalgekar VM (1994). Effects of mass transfer on flow past an impulsively started in finite vertical plate with constant heat flux and chemical reaction, *ForschungimIngenieurwesen*, 60(10), pp. 284-287.
- [16] Manivannan K, Muthucumaraswamy R, Venu T (2009). Radiation and chemical reaction effects on isothermal vertical oscillating plate with variable mass diffusion, *Thermal Science*, 13(2), pp. 155-162.
- [17] Reddy, J.N. 1985. *An Introduction to the Finite Element Method*. McGraw-Hill, New York.
- [18] Bathe, K.J. 1996. *Finite Element Procedures*. Prentice-Hall, New Jersey.

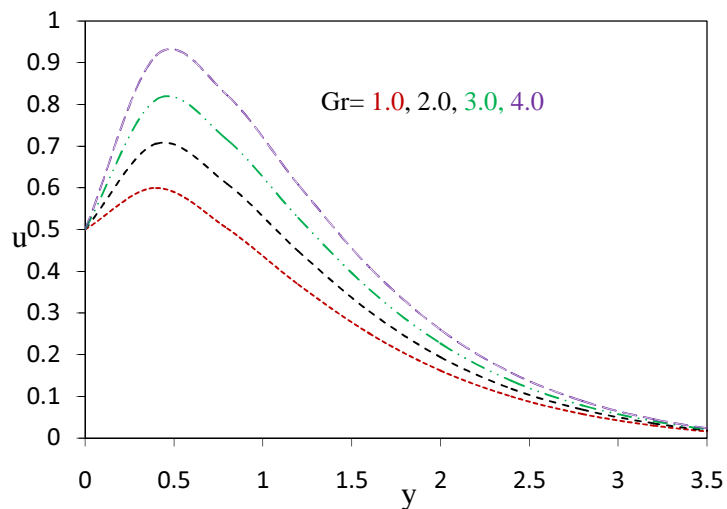


Figure 1. Velocity profiles against  $y$  for different values of  $Gr$

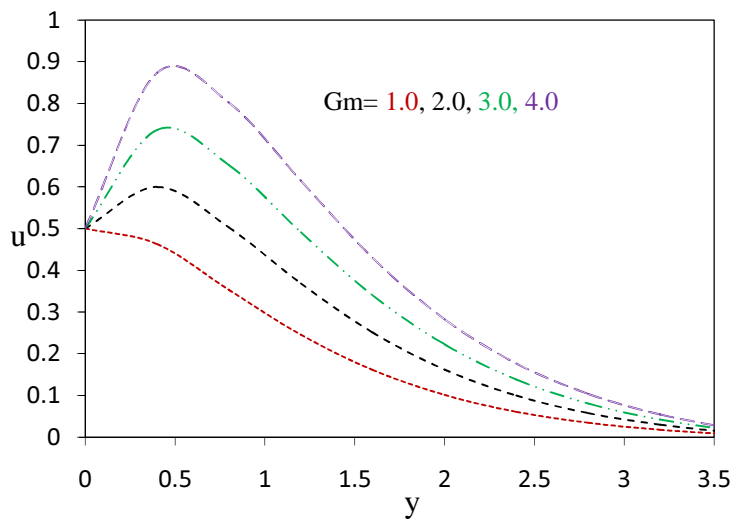


Figure 2. Velocity profiles against  $y$  for different values of  $Gm$

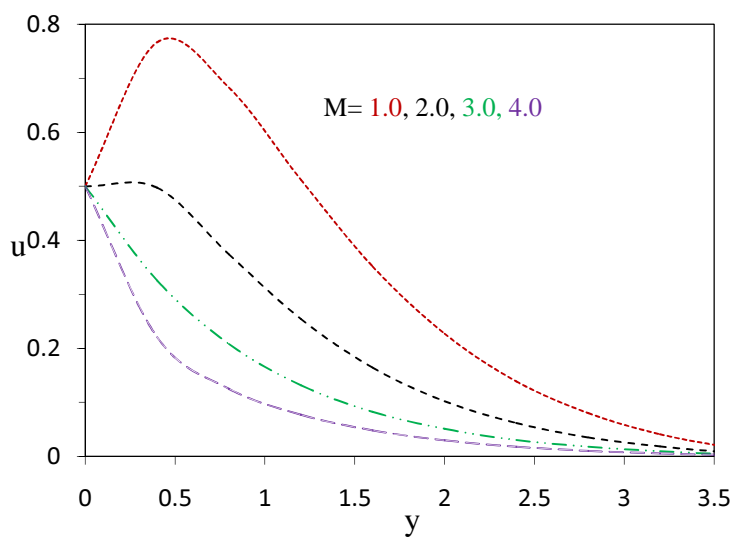


Figure 3. Velocity profiles against  $y$  for different values of  $M$

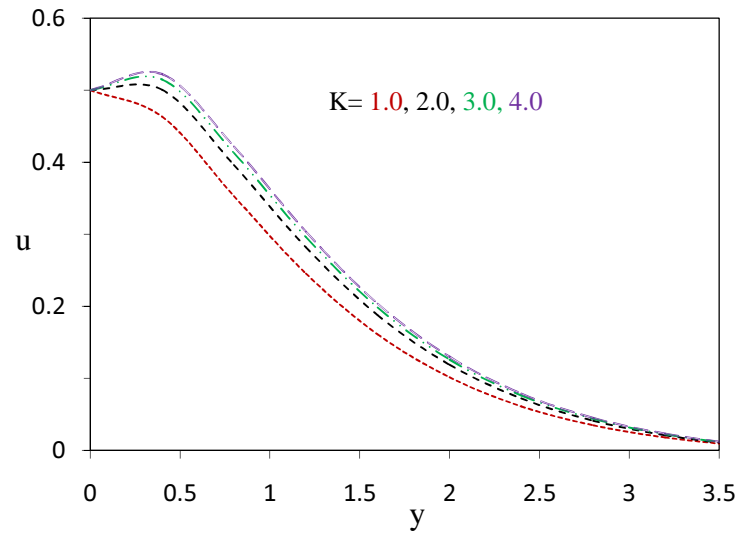


Figure 4. Velocity profiles against  $y$  for different values of  $K$

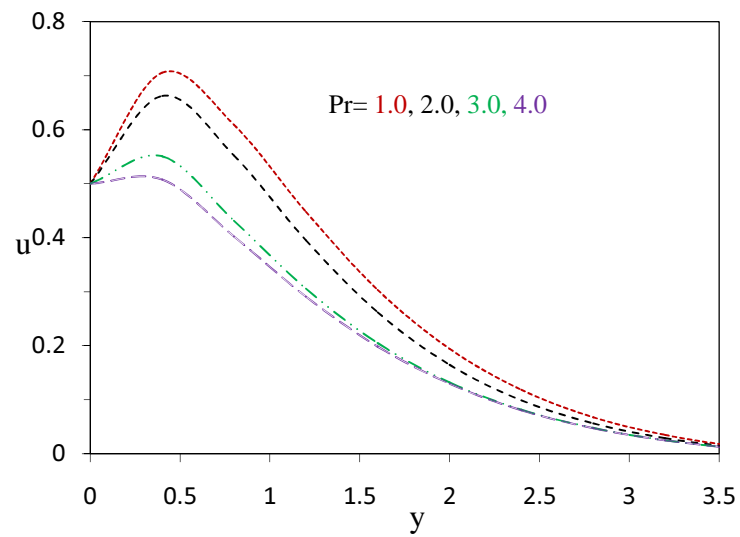


Figure 5. Velocity profiles against  $y$  for different values of  $Pr$

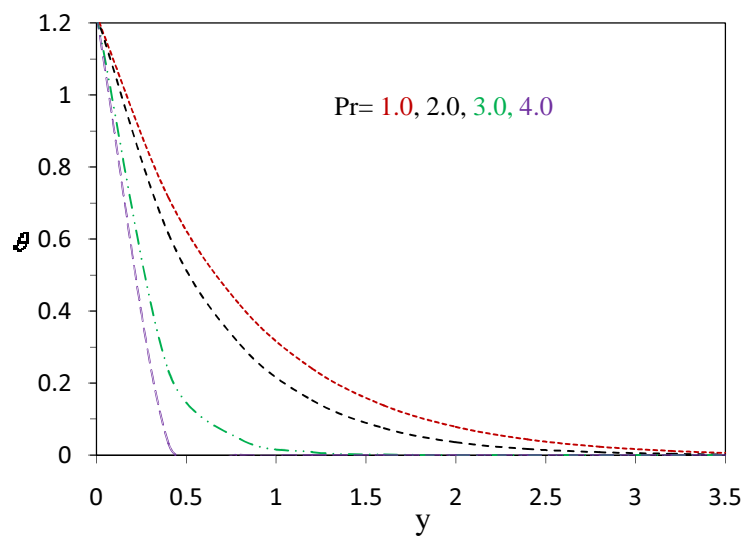


Figure 6. Temperature profiles against  $y$  for different values of  $Pr$

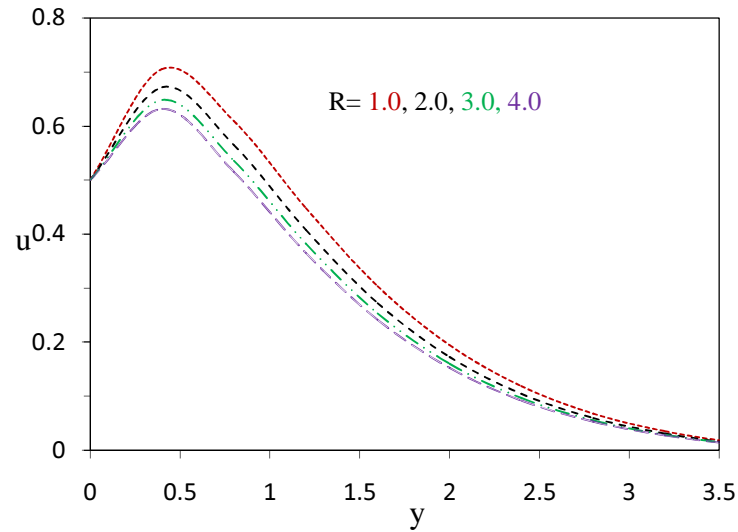


Figure 7. Velocity profiles against  $y$  for different values of  $R$

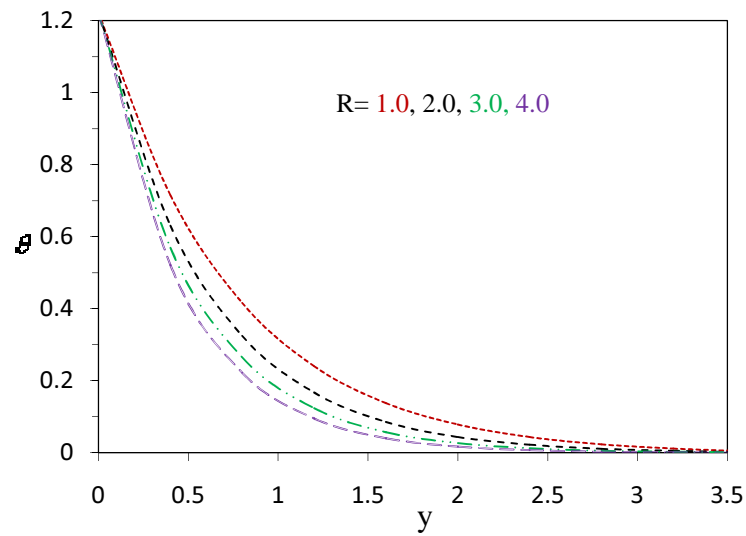


Figure 8. Temperature profiles against  $y$  for different values of  $R$

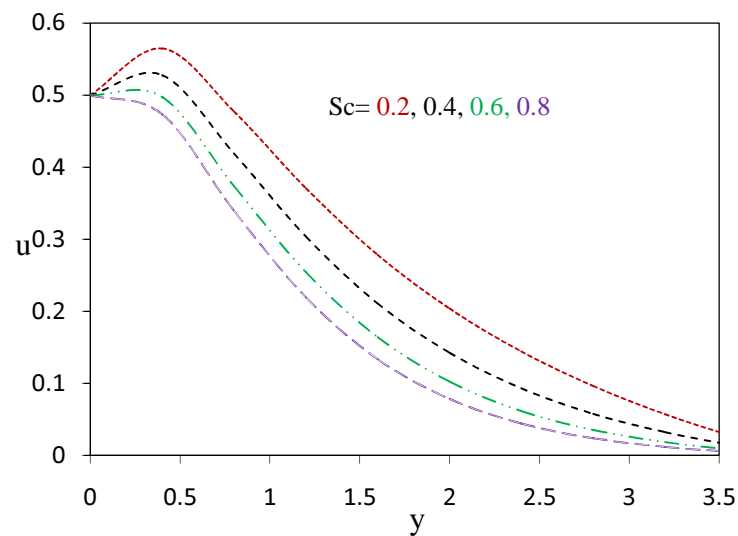


Figure 9. Velocity profiles against  $y$  for different values of  $Sc$

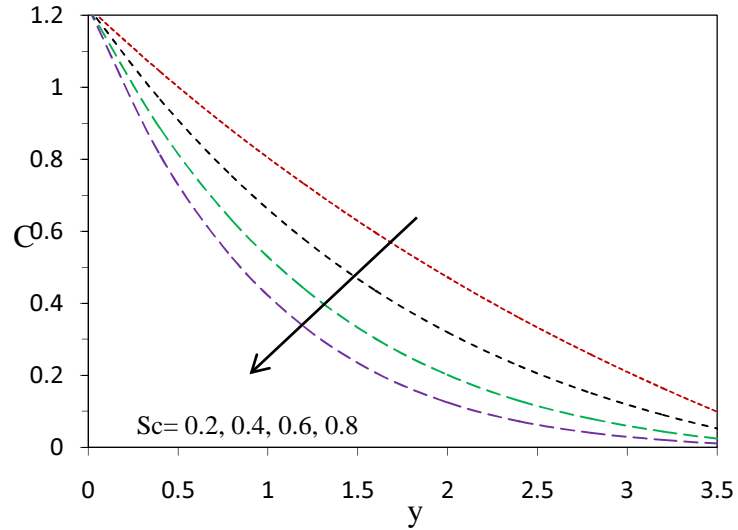


Figure 10. Concentration profiles against  $y$  for different values of  $Sc$

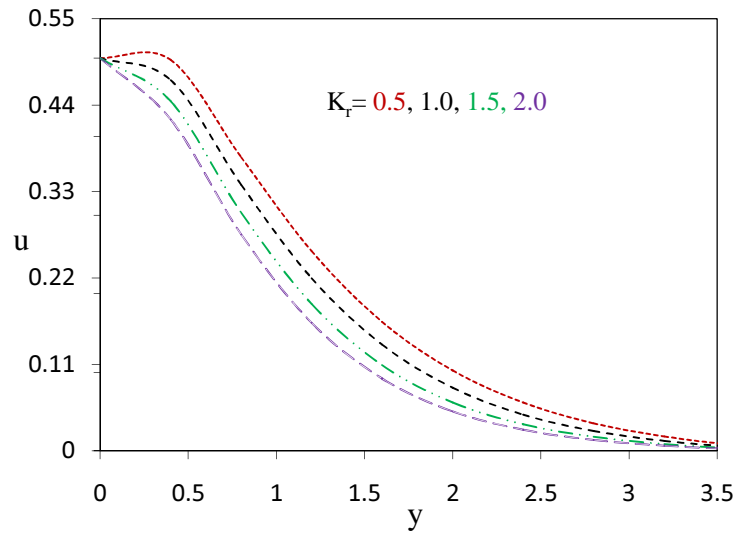


Figure 11. Velocity profiles against  $y$  for different values of  $K_r$

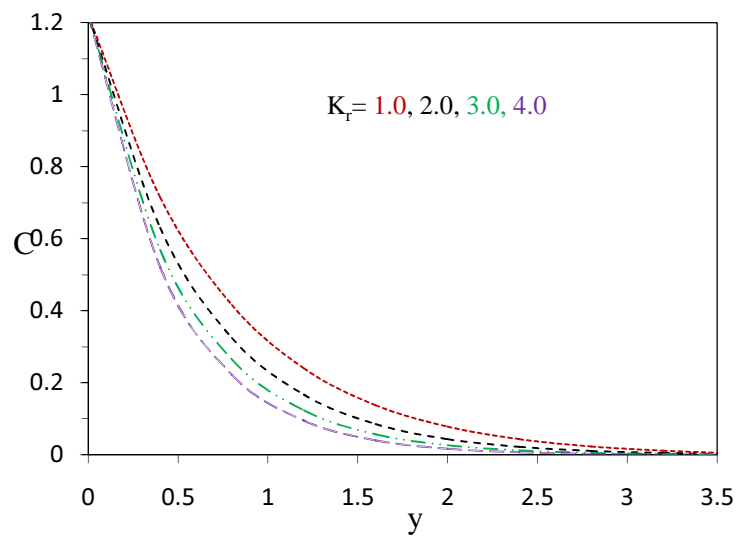


Figure 12. Concentration profiles against  $y$  for different values of  $K_r$